Coaxial jets with and without swirl

By M. M. RIBEIRO† AND J. H. WHITELAW

Department of Mechanical Engineering, Imperial College, London

Measured values of mean velocity, Reynolds stresses and probability density distributions of fluctuating velocity are reported for the turbulent coaxial jets, with and without swirl, emerging into stagnant surroundings from a long pipe and an annulus concentric with the pipe. They were obtained using hot-wire anemometry and on-line data processing with the aid of a mini-computer. The results show that non-swirling coaxial flow configurations approach a self-similar state in a much smaller distance than that of the round jet, for velocity ratios ranging between 0·65 and 1·5; this is due to the mixing layer and vortex shedding that occur in the region downstream of the separation wall between the two streams. In the presence of swirl, the coaxial jet was found to develop at a faster rate. An assessment of turbulence models, based on Reynolds stress closures, suggests that previous assumptions for turbulent diffusion of turbulent kinetic energy are in error.

1. Introduction

The present work is concerned with turbulent flow in the developing region of coaxial axisymmetric free jets with and without swirl. The practical importance of these flow configurations stems from their application in many engineering devices, such as industrial burners, ejectors, jet pumps, where the turbulent mixing of the two coaxial streams is often of primary importance to the efficiency of such devices. In the upstream region, the flow comprises two cores, which result from the pipe and annular flows, and a mixing region between the two streams. It is characterized by considerable turbulent production and the two streams separating from both sides of the inner pipe wall originate two interacting vortex sheets in opposite directions and provide conditions for the occurrence of vortex shedding. When swirl is imparted to the outer stream, the initial region is further complicated by the centrifugal effects that follow the disappearance of the outer pipe wall and establish a rapidly changing radial pressure gradient.

Non-swirling coaxial jet systems have previously been investigated by, for example, Forstall & Shapiro (1950), Chigier & Beer (1964) and Chriss & Paulk (1972) who reported mean velocity profiles obtained with Pitot tubes. Chigier & Beer's work is concerned with the developing region and gives special relevance to the average streamline distribution downstream of the separating wall. Chriss & Paulk were primarily concerned with the behaviour further downstream and give little emphasis to the upstream region.

Measurements of time-averaged tubulence quantities, in addition to mean velocity,

† Permanent address: Instituto Superior Técnico, Lisbon, Portugal.

are reported by Champagne & Wygnanski (1970), Durão & Whitelaw (1973), Matsumoto, Kymoto & Tsuchimoto (1973) and Ribeiro & Whitelaw (1976). These workers present detailed information of the distribution of turbulence properties and provide a basis for the understanding of the influence of the initial velocity ratio on the development of the flow. In addition, Matsumoto *et al.* draw attention to the importance of the region downstream of the separation wall between the two streams in the turbulent mixing, but their investigation only covers the region where $x/D < 4$. Ribeiro & Whitelaw reported measurements for a velocity ratio of one, and give particular emphasis to the region downstream of the inner pipe wall where they detected the occurrence of vortex shedding.

Experimental work in swirling coaxial jets is virtually non-existent. Related work in single jets was reported by Rose (1962), who presented measurements of the mean velocity components and of one of the Reynolds normal stresses in the swirling jet that emerged from a rotating pipe. The works of Craya & Darrigol (1967), Chigier & Chervinsky (1967) and Kawaguchi & Sato (1971) also deal with turbulent swirling jets. Chigier & Chervinsky used a five-hole impact probe to measure the distributions of mean velocity and static pressure. In the other two works, additional information on the Reynolds stress distributions was obtained with hot-wire anemometry. The swirling jet emerging from an annular nozzle was investigated by Chigier & Beer (1964) who reported measurements of mean velocity and static pressure.

The previously available information on the turbulence structure of coaxial jet flows, and particularly those with swirl, does not provide a thorough knowledge of the transport process and is insufficient to allow a satisfactory appraisal of the assumptions made in present-day methods for representing turbulent flows. In this last connexion, it is necessary to postulate and support closure assumptions to approximate the behaviour of unknown quantities in transport equations for correlations of fluctuating velocity components. The latter are assumed to be locally determined and, since a 'model' cannot be universal, the physical plausibility of the inherent assumptions is of great importance.

The major objective of the present work is to obtain measurements, in coaxial jet flows with and without swirl, that will improve understanding of the relevant physical processes. The coaxial flow arrangement and instrumentation used to achieve this purpose are described in the following section. The measurements, which include mean velocity, Reynolds stresses and probability distributions of velocity for zero swirl and three velocity ratios and for a swirl number of 0·26 and one velocity ratio, are presented in § 3. Discussion and concluding remarks are presented in a final section where particular attention is given to the assumptions embodied in proposals for turbulence-model closures of the time or ensemble average hierarchy of equations of motion.

2. Experimental apparatus and procedure

2.1. *Description of flow configuration and initial conditions*

The flow rig used in this work was similar to that used by Durão (1971) and Ribeiro (1972) and a complete description can be found in the first of these works. The exit-plane arrangement, together with the measuring stations and related nomenclature, is shown on figure 1.
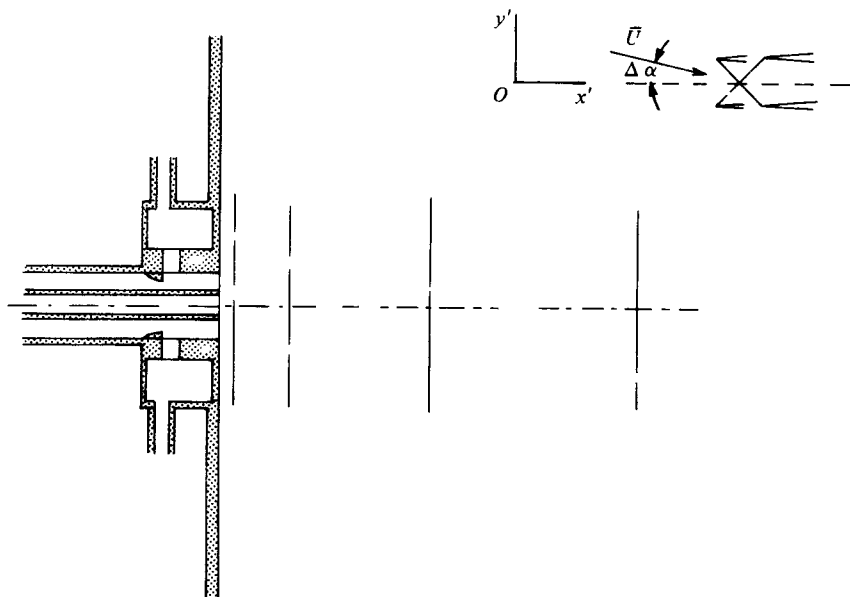
FIGURE 1. Arrangement of coaxial jet. Vertical lines represent measurement stations.

Two separate centrifugal fans delivered armospheric air, through electrostatic filters, to two independent settling chambers which supplied two concentric pipes. The inner pipe was 2·83 m long and had an inner diameter of 1·61 cm and an outer diameter of 2·16 cm; the outer pipe was 2·00 m long and 4·49 cm in inside diameter; the length of the pipes assured fully-developed pipe and annular flows at the exit plane. The relative positioning of the two pipes was achieved through two sets of three blades that could be moved in a direction perpendicular to the inner pipe wall; each set of blades was part of a block rigid with the outer pipe. A solid smooth wall 2·5 m × 2·5 m was located in the exit plane to guarantee a symmetric pattern for the entrained air in the initial region. The whole test region was surrounded by a cage 2 m × 2 m × 5 m, with a $\frac{1}{16}$ in. mesh, to minimize the possible influence of draughts without affecting the entrainment of the surrounding air.

The apparatus was arranged to accommodate swirl in the annular flow by replacing a portion of the outer pipe, near the exit plane, with a swirl chamber which generated a tangential velocity by the injection of air through six equal spaced 4·0 cm × 0·2 cm tangential slots of length 2·0 cm, located at the outer wall 7 cm upstream from the exit. The swirling flow was protected against impingement of the axial stream by the insertion of a backward-facing step immediately upstream of the slots; this also improved the axial symmetry of the flow, owing to the higher residence time of the tangential flow inside the annulus. The axial symmetry of the flow was quantified by measuring two complete radial traverses, in the horizontal and vertical directions, of the mean velocity at 0, 1, 4 and 8 diameters downstream of the inlet. The geometry was considered to be symmetrical when the deviations between the four resulting radial profiles at each station were not larger than 1 % of the centre-line velocity.

The measurements obtained in the absence of swirl correspond to three values of the ratio between the peak velocities at the pipe and annular exit planes, $\bar{U}_i/\bar{U}_o$; these

Velocity ratio $(\bar{U}_i/\bar{U}_o)$	Re_i	Re_o
0·65	25 600	58 900
1·00	31 300	46 800
1·48	41 000	41 500

TABLE 1

values are shown in table 1, together with values of the initial Reynolds numbers based on the average velocities at the outlets of the pipe (Re_i) and of the annulus (Re_o).

For the swirling-flow measurements, the inlet conditions were:

$$\text{velocity ratio} = 0·71, \quad Re_i = 27\,700, \quad Re_o = 53\,900, \quad S = 0·26.$$

The swirl number S, which is a measure of the ratio between the axial flow rates of angular and axial momentum, was calculated according to

$$S = \frac{\displaystyle\int_0^\infty r^2 \bar{U} \bar{V}_\theta \, dr}{R_0 \displaystyle\int_0^\infty r(\bar{U}^2 - \tfrac{1}{2}\bar{V}_\theta^2) \, dr}$$

where R_0 is the radius of the outer pipe and $\bar{U}$ and $\bar{V}_\theta$ are the components of mean velocity in the axial and tangential directions respectively. The influence of the turbulence terms on the value of S has been neglected on the grounds that their contribution, at the inlet station, to the radial integrals of the axial and angular momentum is negligible compared with the mean flow contribution.

2.2. *Hot-wire and data-processing equipment*

The signal-processing instrumentation was identical to that described by Ribeiro & Whitelaw (1975). The signals from a crossed hot-wire probe (DISA 55A32) were passed to linearizers (DISA 55D10) through constant temperature anemometers (DISA 55D01). The voltage signals from the linearizers were supplied to sample-and-hold units (Burr Brown SHM 40) which, in turn, were controlled and sampled by a small computer (Digital PDP8E). This sampling arrangement permitted measurements to be obtained at a frequency of 20 kHz. Processing was achieved in real time; converged averages were obtained after sampling for around 100 to 300 seconds which, in all cases, was at least one order of magnitude greater than the characteristic period of the energy-containing eddies.

The transform equations linking the velocity and signal-voltage characteristics are discussed in detail by Ribeiro (1976) and by Ribeiro & Whitelaw (1975) and are not repeated here. They are similar to those reported and used by Champagne & Sleicher (1967) and are increasingly inappropriate as turbulence-intensity values exceed around 15 %.

In the measurements involving swirl, the mean flow direction is dependent on the location. This introduces two further unknowns and, at each location, two more measurements have to be made. Since practical limitations of hot-wire anemometry imply that the probe axis must coincide with the mean flow direction if a reasonable

level of accuracy is to be achieved, the direction of the flow was determined using a 45°
slanting sensor hot wire prior to taking the measurements that allowed the determina-
tion of the mean velocity and Reynolds stresses. When a 45° probe is located in an
arbitrary plane $Ox'y'$, and the angle between the component of the mean velocity and
the normal to the sensor in $Ox'y'$ differs from $\frac{1}{4}\pi$ by $\Delta\alpha$, the value of the effective cooling
velocity $(\overline{U}_{\text{eff}})_1$ is related to the local mean velocity $\overline{U}$ by (neglecting the influence
of the Reynolds shear stress on the mean value)

$$(\overline{U}_{\text{eff}})_1 = \overline{U}[\cos^2(\tfrac{1}{4}\pi + \Delta\alpha)(\cos^2\beta + h^2\sin^2\beta) + k^2\sin^2(\tfrac{1}{4}\pi + \Delta\alpha)]^{\frac{1}{2}}. \tag{1}$$

$(U_{\text{eff}})_1$ is defined as the velocity normal to the wire which would produce the same
electrical signal from the anemometer as the actual mean velocity. β is the angle
between the plane $Ox'y'$ and the plane defined by the wire and the mean velocity vector.
k is a constant inserted to account for the cooling by the velocity component tangential
to the wire (e.g. see Hinze 1959), and has typical values smaller than 0·2 for the probes
used. h is a constant slightly larger than 1·0 and accounts for the influence of the shape
and dimensions of the probe on the mean flow pattern around the wire (e.g. see Rodi
1971).

If the wire is subjected to a rotation of π around its axis, the value of the effective
cooling velocity becomes

$$(\overline{U}_{\text{eff}})_2 = \overline{U}[\cos^2(\tfrac{1}{4}\pi - \Delta\alpha)(\cos^2\beta + h^2\sin^2\beta) + k^2\sin^2(\tfrac{1}{4}\pi - \Delta\alpha)]^{\frac{1}{2}}. \tag{2}$$

Thus the axis of the probe can be aligned with the mean velocity component in the
$Ox'y'$ plane by rotating the probe around an axis perpendicular to $Ox'y'$ till the mean
value of the signal becomes unchanged by a rotation of π around the probe axis. When
the process is repeated for the plane normal to $Ox'y'$, the mean flow direction is then
determined.

The accuracy of the measurement of the two angles can be estimated as follows.
Assuming $\Delta\alpha$ small and neglecting higher-order terms in (1),

$$\overline{U}_{\text{eff}} \simeq \overline{U}\cos(\tfrac{1}{4}\pi). \tag{3}$$

Upon rotation, the change in effective cooling is

$$\Delta\overline{U}_{\text{eff}} \simeq \overline{U}[\cos(\tfrac{1}{4}\pi + \Delta\alpha) - \cos(\tfrac{1}{4}\pi - \Delta\alpha)] \tag{4}$$

and
$$\Delta\overline{U}_{\text{eff}}/\overline{U}_{\text{eff}} \simeq 2\tan(\tfrac{1}{4}\pi)\Delta\alpha. \tag{5}$$

As a variation of 1 % in $\overline{U}_{\text{eff}}$ can be detected by the measuring system,

$$\Delta\alpha = \frac{0\cdot01}{2\tan(\tfrac{1}{4}\pi)} \simeq 0\cdot3°.$$

Therefore any misalignment between the probe stem and the mean flow direction
greater than 0·3° is detected.

2.3. *Traversing mechanism*

The traversing mechanism included a compound table located on a lathe bed which
allowed displacements in the axial direction. The compound table allowed displace-
ments in two directions in an horizontal plane, with an accuracy of 0·025 mm. Radial
displacements in the vertical direction were achieved by a cathetometer mounted on
the compound table; the maximum travel was 50 cm, with an accuracy of 0·02 mm.

The probe holder allowed rotation of the probes in vertical and horizontal planes. The probe support and the probe holder were connected through a device that allowed rotation of the probe around its axis; a choice of eight different and equally spaced orientations for the plane defined by the sensing wire and the stem axis was available for the same orientation of the probe stem. The measurement of the angles was made with an error not exceeding $0.3°$, which was compatible with the accuracy expected from the processing equipment.

The alignment of the traversing mechanism with the axis of the geometry was obtained with the use of a telescope mounted on a cathetometer at the rear of the plenum chamber; a glass window fitted on the plenum allowed accurate positioning of the probe with the centre-line direction. Disturbances introduced by the probe holder were kept to a minimum by avoiding the presence of the flat surfaces perpendicular to the mean velocity.

3. Measurements and discussion

3.3. *Presentation and analysis of the results for coaxial jet without swirl*

The measurements obtained for the three sets of initial conditions without swirl are presented in the following two subsections. The first deals with the behaviour of the mean velocity and Reynolds stress components along the centre-line and in cross-sectional planes at values of x/D of 0.3, 1, 3 and 6. This is followed by the presentation and discussion of the results obtained for the two-dimensional probability density distributions of the velocity fluctuations.

(a) *Mean velocity and Reynolds stresses.* Figure 2 shows the centre-line distributions of the inverse of the mean velocity and of the Reynolds normal stresses for the three different velocity ratios investigated. The annular flow does not influence the mean velocity at the centre-line inside the first three diameters; it does, however, slightly affect the Reynolds stresses, especially $\overline{v_r^2}$. Between three and six diameters, the centre-line decay of mean velocity asymptotes to a value which is inversely proportional to the distance from the inlet, and the axial normal stress $\overline{u^2}$ is particularly large for the inlet velocity ratio of 0.65; the latter feature is a consequence of large production due to the positive radial mean velocity gradient on the inner side of the outer regime. After six diameters, the profiles of $\overline{u^2}$ and $\overline{v_r^2}$ follow a trend towards self-similarity; for the velocity ratio of 0.65, however, this tendency is slowed by the existence of a flat central region in the radial distributions of mean velocity. At fifteen diameters, the behaviour of the mean flow and of the Reynolds stresses is no longer dependent on the initial conditions.

Figure 3 shows the radial distributions of the mean velocity and Reynolds stresses near the inlet region ($x/D = 0.20$). The axial normal stress, $\overline{u^2}$ still exhibits a double peak in the region of the inner pipe wall but the distribution of $\overline{v_r^2}$ does not. Also in this region, $\overline{v_r^2}$ is always higher than $\overline{u^2}$ and their ratio is a maximum for unity velocity ratio. This results from vortex shedding in the wake of the inner pipe wall but, since the level of Reynolds shear stress is increased, so is the production of $\overline{u^2}$. However $\overline{u^2}$ is still lower than $\overline{v_r^2}$ and the levels of stresses cannot, therefore, be locally determined. It will be shown later than an important effect in this region is radial transport by the radial velocity fluctuations.
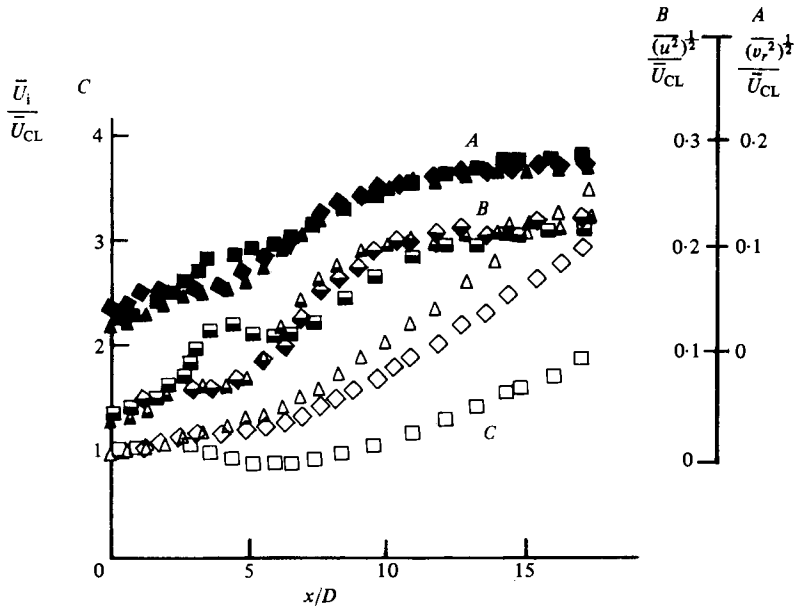
FIGURE 2. Centre-line distributions of mean velocity, axial and radial turbulence intensities; no swirl.

$\overline{U}_i/\overline{U}$	$\overline{U}_i/\overline{U}_{CL}$	$(\overline{u^2})^{\frac{1}{2}}/\overline{U}_{CL}$	$(\overline{v^2})^{\frac{1}{2}}/\overline{U}_{CL}$
1·48	△	◮	▲
1·00	◇	◆	◆
0·65	▢	▰	■

At one diameter downstream, the distributions of mean velocity (figure 4) still exhibit a region of positive radial gradient located between two regions of opposite gradient; and the normal stress $\overline{u^2}$ still scales with the local mean velocity except in a region between $r/R \simeq 0.3$ and $r/R \simeq 0.6$, which may be interpreted as the boundaries of the mixing region between the pipe and annular regimes. The distribution of $\overline{v_r^2}$ does not show the high magnitude displayed at the initial station and its level is everywhere below that of $\overline{u^2}$. The radial profiles of the Reynolds shear stress, $\overline{uv_r}$, still display two changes in sign, which is in qualitative agreement with the occurrence of the two maxima and a minimum in the mean velocity profiles.

Further downstream, at $x/D = 3$, the mean velocity profiles of figure 5 show that only for the velocity ratio of unity does the gradient cross zero at two points. The Reynolds stresses show an individuality that was not present at the previous stations and suggests that the mixing between the two regimes has reached the centreline: their maxima are located in the outer region at $r/R \simeq 1$.

At six diameters downstream, the velocity profiles of figure 6 display monotonic behaviour with slope, increasing with velocity ratio in the central region and decreasing at the edge. In the central region ($r/x \simeq 0.04$) the higher levels of $\overline{u^2}$ are linked with the higher production associated with the higher velocity gradients for the velocity ratio of 1·48, whereas near the edge the higher velocity gradients are linked with the lower velocity ratio. The distributions of $\overline{v_r^2}$ indicate higher values for the lower velocity ratios and, since the production of $\overline{v_r^2}$ is negligible for all the three velocity ratios and,
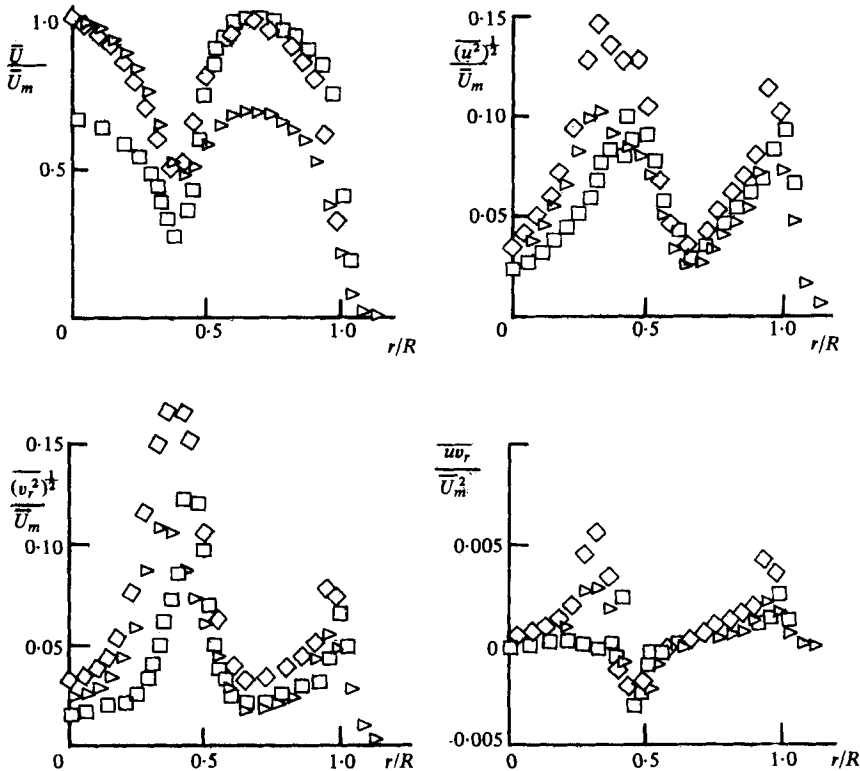
FIGURE 3. Radial profiles of mean velocity, axial and radial turbulence intensities and Reynolds shear stress; no swirl. $x/D = 0.20$. $\overline{U}_i/\overline{U}_o$ values: $\triangleright$, 1.48; $\diamondsuit$, 1.00; $\square$, 0.65. $\overline{U}m$ is the maximum velocity ($= \overline{U}m\ (x)$).

at least in the central region, the expected result of redistribution effects would have an opposite effect to the tendency displayed, it appears that the magnitude of $\overline{v_r^2}$ is determined by turbulent diffusion. The behaviour of the Reynolds shear stress already exhibits the same trend as a fully-developed jet.

The radial profiles of mean velocity and the Reynolds stresses $\overline{u^2}$, $\overline{v_r^2}$ and $\overline{uv_r}$, at $x/D = 10$ and 15 are not reproduced here for reasons of space; they have been presented by Ribeiro (1976). The mean velocity profiles are undistinguishable from self-similarity but the Reynolds stresses are slightly lower than those expected for the self-similar cases. At the centre-line, for example, $(\overline{u^2})^{\frac{1}{2}}/\overline{U}_{\mathrm{CL}} \simeq 0.21$, $(\overline{v_r^2})^{\frac{1}{2}}/\overline{U}_{\mathrm{CL}} \simeq 0.17$ and the shear stress reaches a maximum at $r/x \simeq 0.06$, with a value of $\overline{uv_r}/\overline{U}_{\mathrm{CL}}^2 \simeq 0.012$.

(b) *Probability density distributions.* The probability density distributions of the velocity fluctuations were measured in a two-dimensional velocity space and, therefore, may be interpreted as the result of integration of the three-dimensional distributions, $f(\mathbf{v})$, over the uni-dimensional space of the third velocity component. The two dimensions concerned are the axial, u, and radial, v_r, components of the velocity fluctuations. The probability density distribution, $f(u, v_r)$ satisfies the following relationships:

$$f(u, v_r) = \int_{V_\theta} f(\mathbf{v})\, dv_\theta, \tag{6}$$
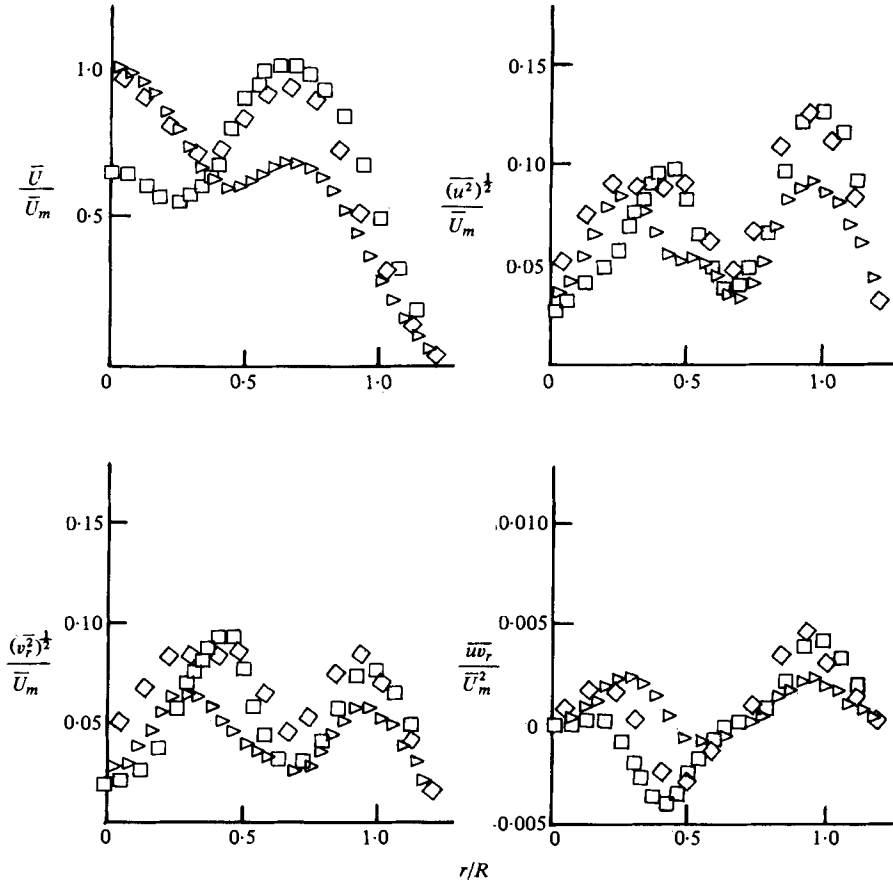
FIGURE 4. Radial profiles of mean velocity, axial and radial turbulence intensities and Reynolds shear stress; no swirl. $x/D = 1\cdot00$. Legend as for figure 3.

$$\int_{V_r} f(u, v_r)\, dv_r = f(u), \tag{7}$$

$$\int_{U} f(u, v_r)\, du = f(v_r), \tag{8}$$

$$\int_{U} \int_{V_r} f(u, v_r)\, du\, dv_r = 1, \tag{9}$$

where $f(u)$ and $f(v_r)$ are the uni-dimensional distributions of the axial and radial velocity fluctuations. It is presented in the non-dimensional form obtained when normalized by its standard deviations, σ_u and σ_v, i.e.

$$\sigma_u^2 \equiv \overline{u^2} = \int_{U} \int_{V_r} u^2 f(u, v_r)\, du\, dv_r, \tag{10}$$

$$\sigma_v^2 \equiv \overline{v_r^2} = \int_{U} \int_{V_r} v_r^2 f(u, v_r)\, du\, dv_r \tag{11}$$
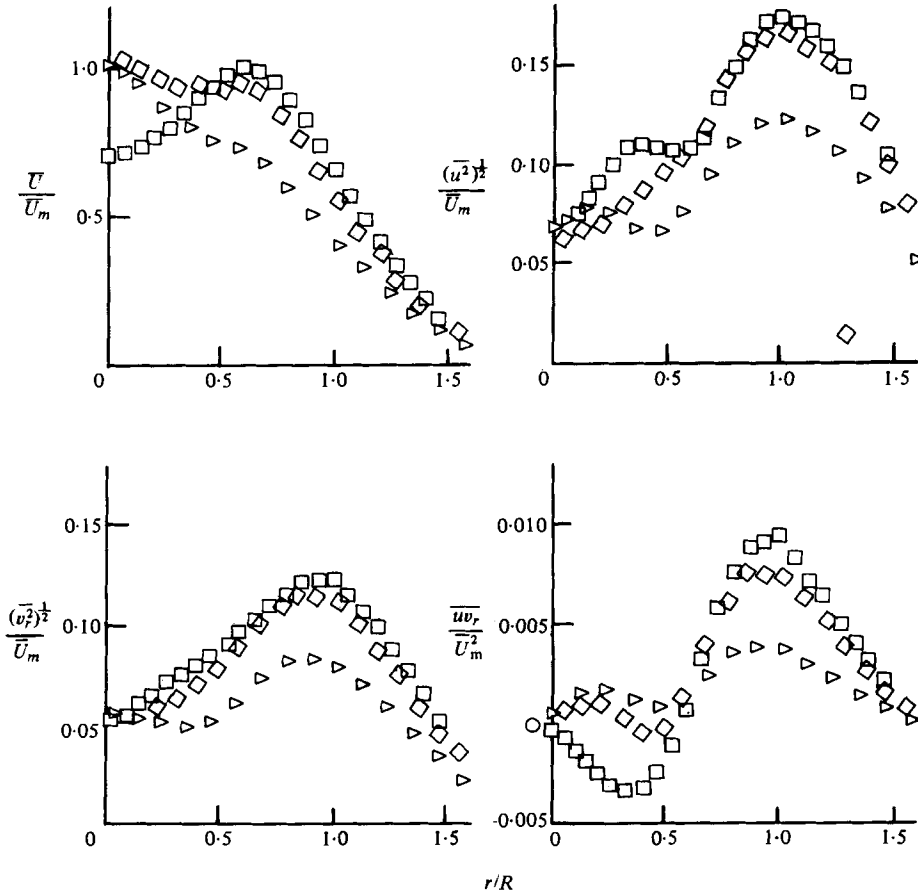
FIGURE 5. Radial profiles of mean velocity, axial and radial turbulence intensities and Reynolds shear stress; no swirl. $x/D = 3.00$. Legend as for figure 3.

and is represented as $B(u, v_r)$. Equation (9) can be rewritten as

$$\int_U \int_{V_r} B(u, v_r)\, d(u/\sigma_u)\, d(v_r/\sigma_v) = 1. \tag{12}$$

$B(u, v_r)$ was examined in two ways: (a) in the form of three-dimensional plots where u/σ_u and v_r/σ_v appeared in an horizontal plane as independent variables and $B(u, v_r)$ as a dependent variable in the vertical direction; (b) as lines of isoprobability,

$$B(u, v_r) = c,$$

with the values of c given in table 2. In figures 7 and 8, which present some of these results, the convention for the sign of the fluctuations is that for the axial component, u, the positive values correspond to fluctuations above the value of the mean velocity and for the radial fluctuations, v_r, the positive fluctuations are associated with a travel towards the edge of the jet. The ambiguity in the sign of v_r at the centre-line is solved by taking one direction arbitrarily as positive.

$\dfrac{\bar{U}}{\bar{U}_{CL}}$

1·0

0·50

0   0·05   0·10   0·15

$\dfrac{\overline{(u^2)}^{\frac{1}{2}}}{\overline{U}_m}$

0·15

0·10

0·05

0   0·05   0·10   0·15

$\dfrac{\overline{(v_r^2)}^{\frac{1}{2}}}{\overline{U}_m}$

0·15

0·10

0·05

0   0·05   0·10   0·15

$\dfrac{\overline{uv_r}}{\overline{U}_m^2}$

0·010

0·005

0   0·05   0·10   0·15

r/x
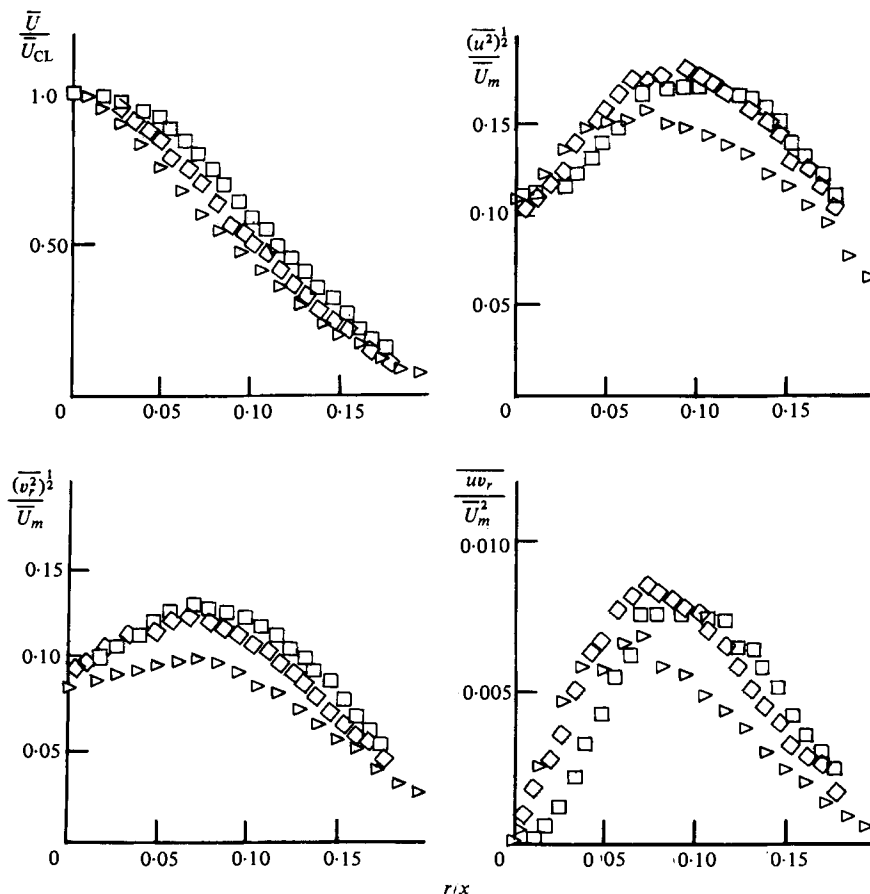
FIGURE 6. Radial profiles of mean velocity, axial and radial turbulence intensities and Reynolds shear stress; no swirl. $x/D = 6\cdot00$. Legend as for figure 3.

Contour	Value of c	Contour	Value of c
1	0·0064	6	0·0784
2	0·0144	7	0·1024
3	0·0256	8	0·1296
4	0·0400	9	0·1600
5	0·0576		

TABLE 2. Values of the probability density for the isoprobability lines of figures 7 and 8. The contours are numbered from the outer to the inner region. Each number refers to a contour that encloses the one with the immediately higher number and is enclosed by the one with the immediately lower number.

In figures 7 and 8, the probability density distributions along the centre-line are presented for the three velocity ratios; three-dimensional plots, obtained in all cases, are presented on figure 7 only and for demonstration purposes. The deviations from symmetry around the u axis reflect inaccuracy of the measurements since axial symmetry implies a symmetric distribution around the u axis. In all figures except 7 (*b*), i.e.
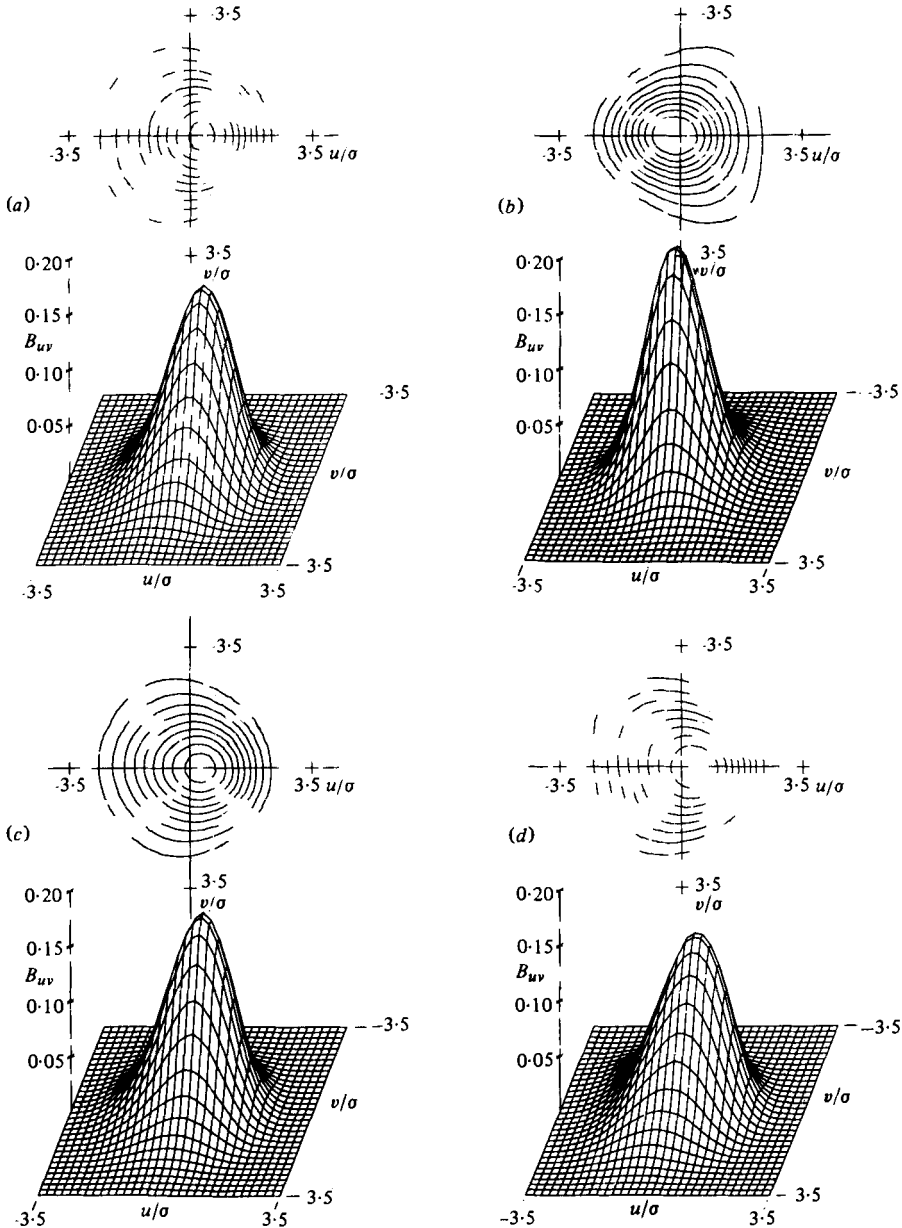
FIGURE 7. Two-dimensional probability density distributions $B(u, v_r)$ along centre-line for velocity ratio $\bar{U}_i/\bar{U}_o' = 0.65$; no swirl. (a) $x/D = 0.2, r/R = 0$; (b) $x/D = 3, r/x = 0$; (c) $x/D = 6$, $r/x = 0$; (d) $x/D = 10, r/x = 0$.

for the lowest velocity ratio and $x/D = 3$, the most probable value for the u fluctuations is positive and the skewness of the u distribution along the centre-line is, therefore, negative. The axial mean velocity gradient is negative everywhere, except in a region between 2.5 and 5 diameters for the lowest velocity ratio (see figure 2). The non-zero skewness results from the dominant occurrence of eddies moving either with a velocity
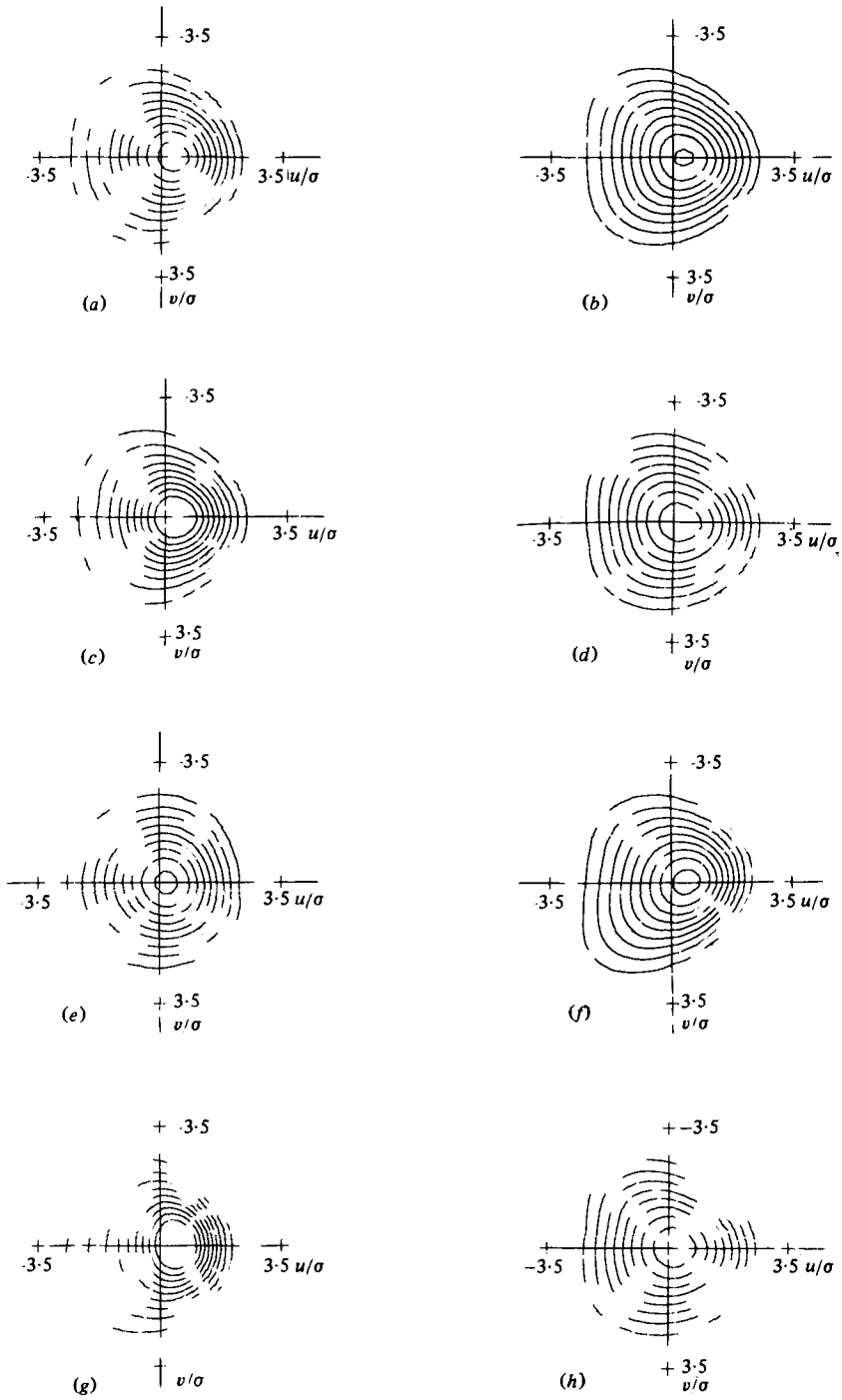
FIGURE 8 (*a–h*). For legend see page 783.
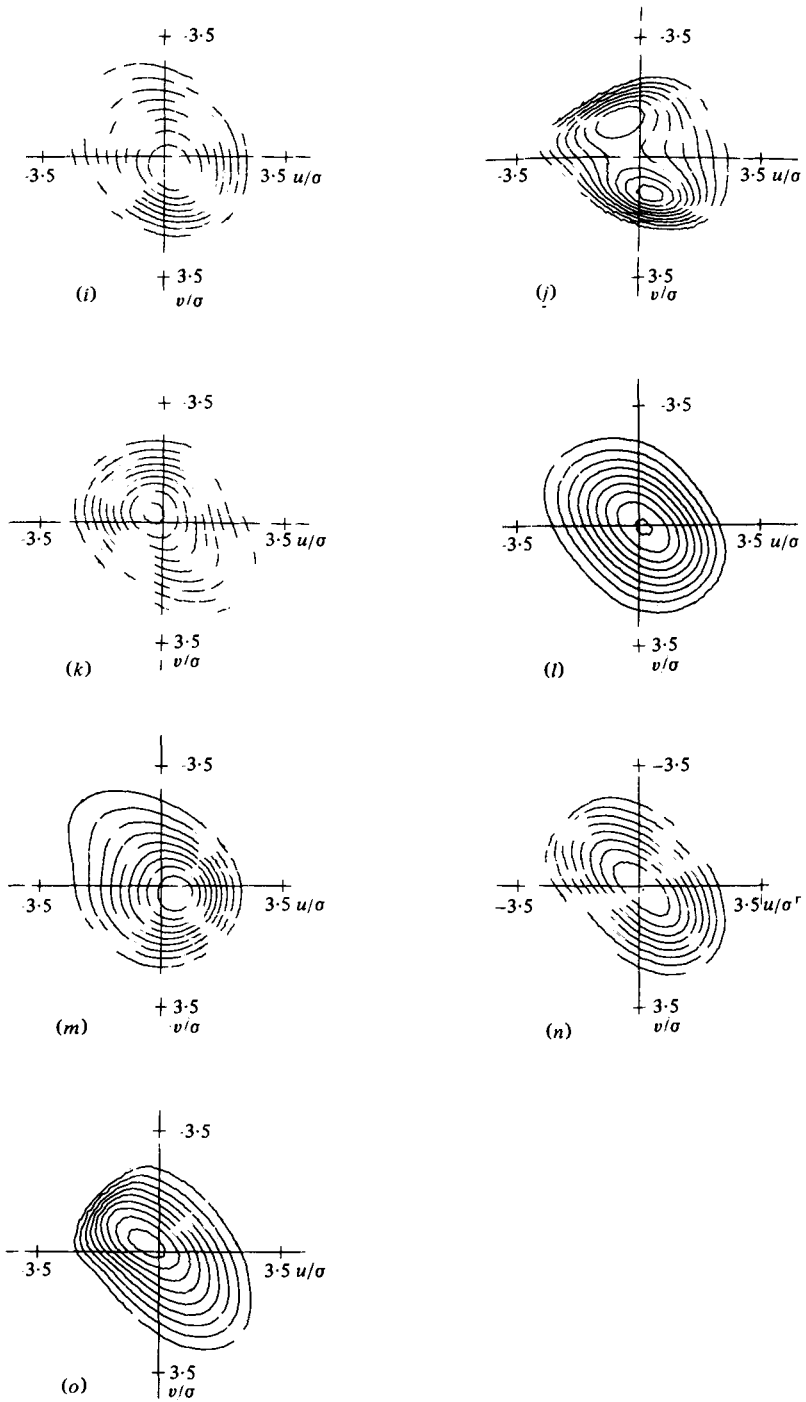
FIGURE 8 (*i–o*). For legend see opposite page.

higher or lower than the local mean velocity and these eddies therefore reflect non-uniform velocity gradients and have non-local origins.

This can be shown to be compatible with the measured probability distributions as follows. Consider a location of the centre-line where $\partial \overline{U}/\partial x < 0$ (e.g. figure 8h). The portion of the volume surrounding this location, where the mean velocity is lower than the local mean, is larger than the portion where the opposite prevails. It can be expected, therefore, that fluctuations with a large radial component have a characteristic velocity that is lower than the local mean. This may be confirmed from the figure which shows positive u's occurring with small v_r's, and negative u's co-existing with a wider range of v_r's. This evidence is consistent with the arguments of Townsend (1956) and Bradshaw, Ferriss & Atwell (1967) which attribute the turbulent diffusion mainly to the large scales.

Figures 8(i), (j) and (k) are typical of results obtained close to the exit plane. Distribution 8(i) refers to a location in the central core where the mean velocity gradient is negative and the Reynolds shear stress is positive. It shows that the value of the shear stress is a result of (i) a preferred direction for the velocity fluctuations and also (ii) of a high probability of occurrence of slow motions ($u < 0$) from the outer regions ($v_r < 0$). A similar pattern is observed in distribution 8(k) which also corresponds to a region where the Reynolds shear stress is positive; the preferred direction is the same as for distribution 8(i), but the value of the stress is enhanced by the occurrence of fast axial motions directed outwards. Distribution 8(j) refers to a location of the inner pipe wall; it is bimodal owing to the occurrence of vortex shedding. Additional measurements in this region have been reported by Ribeiro (1976) who deduced that: (i) vortex shedding occurred for all the velocity ratios considered; (ii) the two peaks in the probability density distribution decay slowly with the axial distance inside a region which covers the first 15 wall thicknesses; (iii) the spacing between the peaks remains essentially the same inside that region and implies that the amplitude of the velocity fluctuations does not change significantly.

The pattern exhibited by figure 8(j) also helps to explain the difference in the radial distributions of the two measured Reynolds normal stresses (see figure 3). Contrary to $\overline{u^2}$, $\overline{v_r^2}$ does not exhibit two maxima in the wake of the inner pipe wall. Distribution 8(j), due to its asymmetry in the v_r dimension, implies that the odd-order moments of v_r will be of large magnitude and, since the turbulent diffusion of $\overline{v_r^2}$ is mainly due to $-\partial(\overline{v_r^3})/\partial r$, it is to be expected that the radial diffusion of $\overline{v_r^2}$ will be large in this region.

Figures 8(l)–8(o) show the probability density distributions at three and six diameters for the velocity ratio of unity. At $x/D = 3$ and close to the centre line where the Reynolds shear stress is positive, the main contribution to the value of the Reynolds shear stress corresponds to a directional preference for the fluctuations, since high values of u tend to co-exist with high values of v_r of opposite sign, for u both positive

FIGURE 8. Two-dimensional probability density distributions $B(u, v_r)$; no swirl. (a) $\overline{U}_i/\overline{U}_o = 1\cdot00$, $x/D = 0\cdot2$, $r/R = 0$; (b) $\overline{U}_i/\overline{U}_o = 1\cdot00$, $x/D = 3\cdot0$, $r/R = 0$; (c) $\overline{U}_i/\overline{U}_o = 1\cdot00$, $x/D = 6\cdot0$, $r/R = 0$; (d) $\overline{U}_i/\overline{U}_o = 1\cdot00$, $x/D = 10\cdot0$, $r/R = 0$; (e) $\overline{U}_i/\overline{U}_o = 1\cdot48$, $x/D = 0\cdot2$, $r/R = 0$; (f) $\overline{U}_i/\overline{U}_o$ $1\cdot48$, $x/D = 3\cdot0$, $r/R = 0$; (g) $\overline{U}_i/\overline{U}_o = 1\cdot48$, $x/D = 6\cdot0$, $r/R = 0$; (h) $\overline{U}_i/\overline{U}_o = 1\cdot48$, $x/D = 10\cdot0$, $r/R = 0$; (i) $\overline{U}_i/\overline{U}_o = 1\cdot48$, $x/D = 0\cdot2$, $r/R = 0\cdot258$; (j) $\overline{U}_i/\overline{U}_o = 1\cdot48$, $x/D = 0\cdot2$, $r/R = 0\cdot378$; (k) $\overline{U}_i/\overline{U}_o = 1\cdot48$, $x/D = 0\cdot2$, $r/R = 0\cdot809$; (l) $\overline{U}_i/\overline{U}_o = 1\cdot00$, $x/D = 3\cdot0$, $r/R = 0\cdot026$; (m) $\overline{U}_i/\overline{U}_o = 1\cdot00$, $x/D = 3\cdot0$, $r/R = 0\cdot100$; (n) $\overline{U}_i/\overline{U}_o = 1\cdot00$, $x/D = 6\cdot0$, $r/R = 0\cdot079$; (o) $\overline{U}_i/\overline{U}_o = 1\cdot00$, $x/D = 6\cdot0$, $r/R = 0\cdot109$.

and negative. Distribution 8 (*m*) refers to the same downstream station, at a location where the mean velocity gradient is small but changing appreciably; there is also a significant contribution of type (ii) for the Reynolds shear stress, due to the distribution being skewed in that particular direction. Since the contributions of type (i) are important where the mean velocity gradient is constant, they may be locally determined. The second type of contribution has the same origin as the third-order velocity correlations and is consistent with non-constant mean velocity gradients and with turbulent transport from regions at a finite distance. This simplistic argument is supported by the fact that, for small values of u and v_r, the isoprobability lines have an approximately elliptic shape which disappears at higher values of the fluctuations.

At six diameters, and at locations where the values of the Reynolds shear stress approach a maximum ($r/x \simeq 0.08$) or where the mean velocity reaches half the centre-line value ($r/x \simeq 0.109$), the distributions are similar to those of Ribeiro & Whitelaw (1975) for the self-preserving region of a single jet. In the region of maximum shear stress, this quantity is probably locally determined, since the isoprobability lines were approximately symmetrical. It should be remembered that the local turbulence level is very high and, as pointed out by Tutu & Chevray (1975), inaccuracies may be expected in the representation of the local instantaneous velocity obtained from the hot-wire sensor. These inaccuracies are mainly due to rectification, and therefore occur when the instantaneous velocity changes sign (i.e. u high in magnitude and negative). In spite of this effect, the pattern shown in distribution 8 (*o*) is consistent with the expected behaviour of the velocity; values of axial momentum higher than the local mean ($u > 0$) are associated with a long travel from the inner regions ($v_r > 0$), while fluctuations with an axial momentum lower than the local mean ($u < 0$) seem to have a local origin ($v_r \simeq 0$) and, therefore, may be interpreted as representing local changes in the instantaneous velocity, i.e. intermittency.

The distributions at ten and fifteen diameters are not shown here and may be found in Ribeiro (1976). The observed pattern shows that, while the values of the Reynolds stresses are still changing in the streamwise direction, the shape of the probability distributions are only dependent on r/x. In view of this apparent self-similarity it is safe to assume that in this region all the moments of distributions, normalized by their standard deviations, are independent of the axial distance and initial velocity ratio.

3.2. *Presentation and analysis of results for co-axial jet with swirl*

(*a*) *Mean velocity and Reynolds stresses.* The distributions of the mean velocity and normal stresses along the centre-line of the swirling flow are shown on figure 9. The ratio of the inlet velocity, $\overline{U}_i$, to the local velocity, $\overline{U}_{CL}$, is linear with the axial distance for distances higher than four diameters and the virtual origin appears to be situated at a negative value of x of around 3.5 diameters upstream from the inlet. There is an expected similarity with the equivalent case without swirl; two main differences are: (i) the swirling flow has a higher spreading rate; (ii) in the initial region ($x/d < 0.3$), the distribution of mean velocity exhibits a much faster decay. This second difference is a direct result of the pressure sink term in the transport equation for the axial momentum. The pressure deficit at the centre-line depends mainly on the radial behaviour of the centrifugal force, $\overline{V_\theta^2}/r$ and, in the region immediately downstream from the inlet, the sudden removal of the confinement imposes a very high rate of
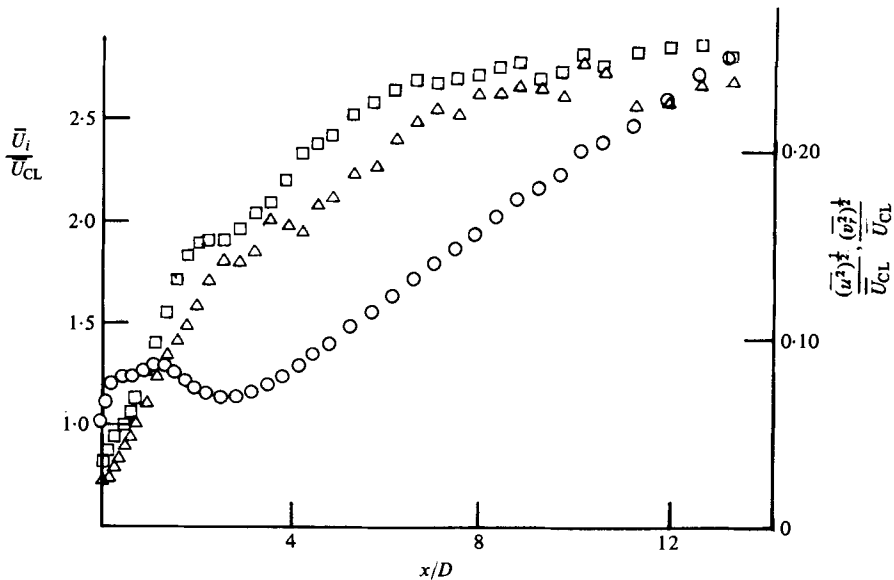
FIGURE 9. Centre-line distributions of mean axial velocity, axial and radial turbulence intensities, swirl number = 0·26. $\bigcirc$, $\bar{U}_i/\bar{U}_{CL}$; $\square$, $(\overline{u^2})^{\frac{1}{2}}/\bar{U}_{CL}$; $\triangle$, $(\overline{v_r^2})^{\frac{1}{2}}/\bar{U}_{CL}$.

change upon the tangential velocity field. The centre-line pressure follows this change and, therefore, a positive axial pressure gradient is established and acts as a sink of mean velocity. The effect lasts until the tangential velocity component readjusts itself to the disappearance of the outer wall. The evolution of the normal stresses along the centre-line is similar to that reported for the non-swirling case.

Figure 10 represents the radial distributions, at the inlet station, of the components of the mean velocity and Reynolds stress tensor. In the inner region ($r/R < 0.36$), the levels of the normal stresses are in agreement with those expected for pipe flow. The annular core, however, exhibits turbulence intensities around 20 %, and these high values are partly attributable to the existence of the upstream backward-facing step and the consequent strong generation and transport of turbulence inside this region. Both the tangential and axial components of mean velocity have nearly linear distributions along the radial direction with maxima near the outer and inner walls, respectively. The levels of the Reynolds shear stresses, $\overline{uv_r}$ and $\overline{uv_\theta}$, are accordingly high and the positive value for $\overline{uv_\theta}$ is due to the clockwise swirl which also causes a negative value for $\bar{V}_\theta$.

Figure 11 refers to a radial station one diameter downstream from the inlet. The axial component of the mean velocity already possesses a flat central region which did not occur in the non-swirling flow until three diameters downstream. The tangential component of the mean velocity has spread into the inner region, and its radial gradient at the centre-line ceased to be zero. The normal stresses in the radial and tangential directions show similar magnitudes and a uniform behaviour along the radius; this feature exists at all the subsequent downstream stations and suggests a strong turbulent diffusion. The axial stress, $\overline{u^2}$, exhibits a less uniform behaviour with a minimum occurring in the wake of the inner pipe wall; this conforms to the pattern obtained in the absence of swirl and can be justified by a lower diffusion for the axial
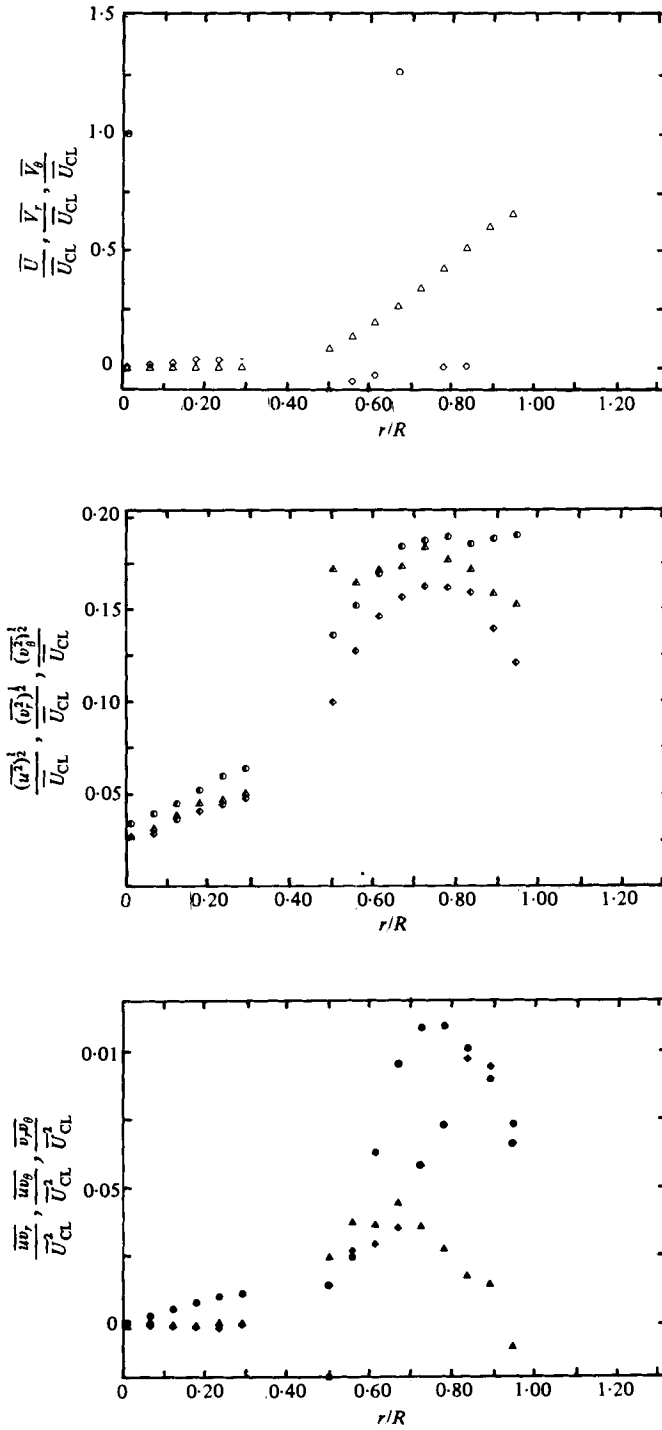
FIGURE 10. Radial profiles of mean velocities, turbulence intensities and Reynolds shear stresses. $x/D = 0.0$, swirl number $= 0.26$; $x/D = 0$. $\bigcirc$, $\bar{U}/\bar{U}_{\mathrm{CL}}$; $\mathbb{C}$, $(\overline{u^2})^{\frac{1}{2}}/\bar{U}_{\mathrm{CL}}$; $\bullet$, $\overline{uv}_r/\bar{U}_{\mathrm{CL}}^2$; $\diamondsuit$, $\bar{V}_r/\bar{U}_{\mathrm{CL}}$; $\blacklozenge$, $(\overline{v_r^2})^{\frac{1}{2}}/\bar{U}_{\mathrm{CL}}$; $\blacklozenge$, $\overline{uv}_\theta/\bar{U}_{\mathrm{CL}}^2$; $\triangle$, $-\bar{V}_\theta/\bar{U}_{\mathrm{CL}}$; $\blacktriangle$, $(\overline{v_\theta^2})^{\frac{1}{2}}/\bar{U}_{\mathrm{CL}}$; $\blacktriangle$, $\overline{v_r v_\theta}/\bar{U}_{\mathrm{CL}}^2$.
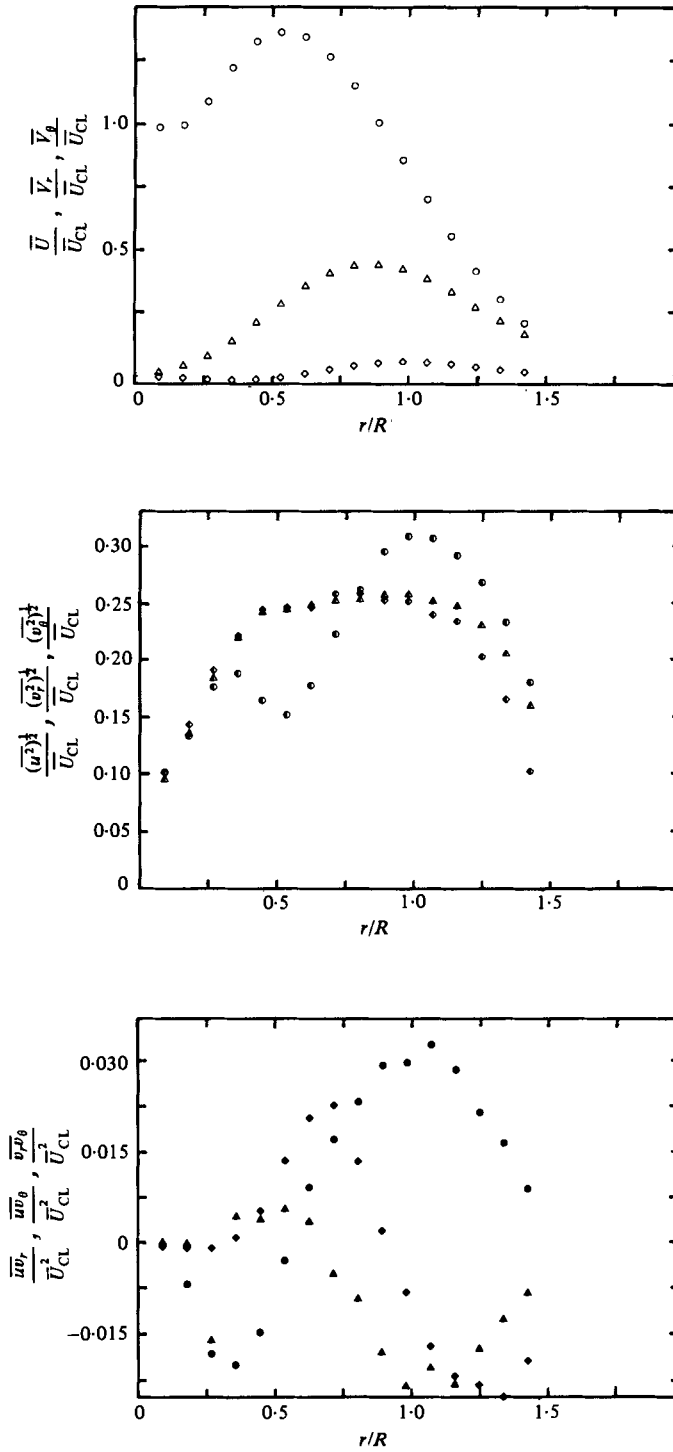
FIGURE 11. Radial profiles of mean velocities, turbulence intensities and Reynolds shear stresses, $x/D = 1.00$, swirl number $= 0.26$. Legend as for figure 10.

stress. The shear stress distributions show that both $\overline{uv_r}$ and $\overline{uv_\theta}$ change signs in the neighbourhood of the location where the maxima for $\overline{U}$ and $\overline{V_\theta}$ occur. The behaviour of $\overline{v_r v_\theta}$ is more complex, since it is dictated by the relative weight of $\overline{V_\theta}$ and its radial gradient, i.e. the production of $\overline{v_r v_\theta}$ may be expressed in the form

$$P(\overline{v_r v_\theta}) \simeq -\overline{v_r^2}\frac{\partial \overline{V_\theta}}{\partial r} + \overline{v_\theta^2}\frac{\overline{V_\theta}}{r}. \tag{13}$$

The two normal stresses are similar and, in regions where $\overline{V_\theta}$ and its gradient have the same sign $(r/R \simeq 0.8)$, their effects tend to cancel each other. For r/R greater than 0.8, both these quantities yield a negative value for $\overline{v_r v_\theta}$ and this is qualitatively confirmed by its measured distribution.

Figure 12 refers to $x/D = 1.5$, where the axial component of mean velocity shows that the size of the central flat core has been considerably reduced and the production of $\overline{u^2}$ in the neighbourhood of the centre-line increased with consequent disappearance of the minimum in the region downstream of the inner pipe wall. A nearly isotropic distribution occurs in the central region, i.e. for r/R less than 0.6. Not only are the normal stresses similar in magnitude but the shear stresses also exhibit very low levels. These quantities increase in magnitude outside this region, and $\overline{uv_r}$ becomes the dominant stress.

At three diameters downstream (figure 13), the maximum axial velocity is on the centre line and the tangential component is very small. The occurrence of a flat central region implies a lower production of $\overline{u^2}$ than in the outer region, where $\overline{u^2}$ is 25 % higher than the other normal stresses. The distribution of the shear stresses shows an increase in $\overline{uv_r}$, relative to the other two, and stems from the dominance of the axial component of mean velocity.

Figure 14 shows the radial distribution of the mean velocity and Reynolds stresses at six diameters where the mean velocity profile is close to fully developed and the normal stresses display much more uniform profiles than in the corresponding flow without swirl.

The above discussion shows that the introduction of swirl is responsible for a considerable increase in the mixing process. The centrifugal forces impose a pressure gradient in the radial direction which increases the rate of spread of the jet. This sets up strong changes in the velocity field, which, in turn, generates turbulence and increases the mixing and the rate of spread. The process appears to be dictated initially by the centrifugal forces, and gradually taken over by the increased turbulent mixing.

(b) *Probability density distributions.* The development of the joint probability density distributions along the centre-line is shown in figure 15. Interpretation of these distributions seems to confirm the existence of a correlation between the behaviour of the mean velocity gradient and the values of the skewness of the distributions in the u direction; at x/D equal to 0 and 6, the skewness and the axial gradient are negative; at $x/D = 2$, both quantities are positive and, at $x/D = 3$, they are both zero. This is in agreement with the findings for the non-swirling case, where these observations suggested a dependence of the turbulent diffusion on the macroscales of the motion.

The values of $B(u, v_r)$ and $B(u, v_\theta)$ at the inlet station and on the edge of the pipe flow $(r/R = 0.3)$ correspond to $\overline{uv_r}$ high and positive and $\overline{uv_\theta}$ zero. The distribution of $B(u, v_r)$ shows that the magnitude of the stress $\overline{uv_r}$ is mainly due to a preferred direction of the fluctuations and, since the distribution does not exhibit high skewness in any
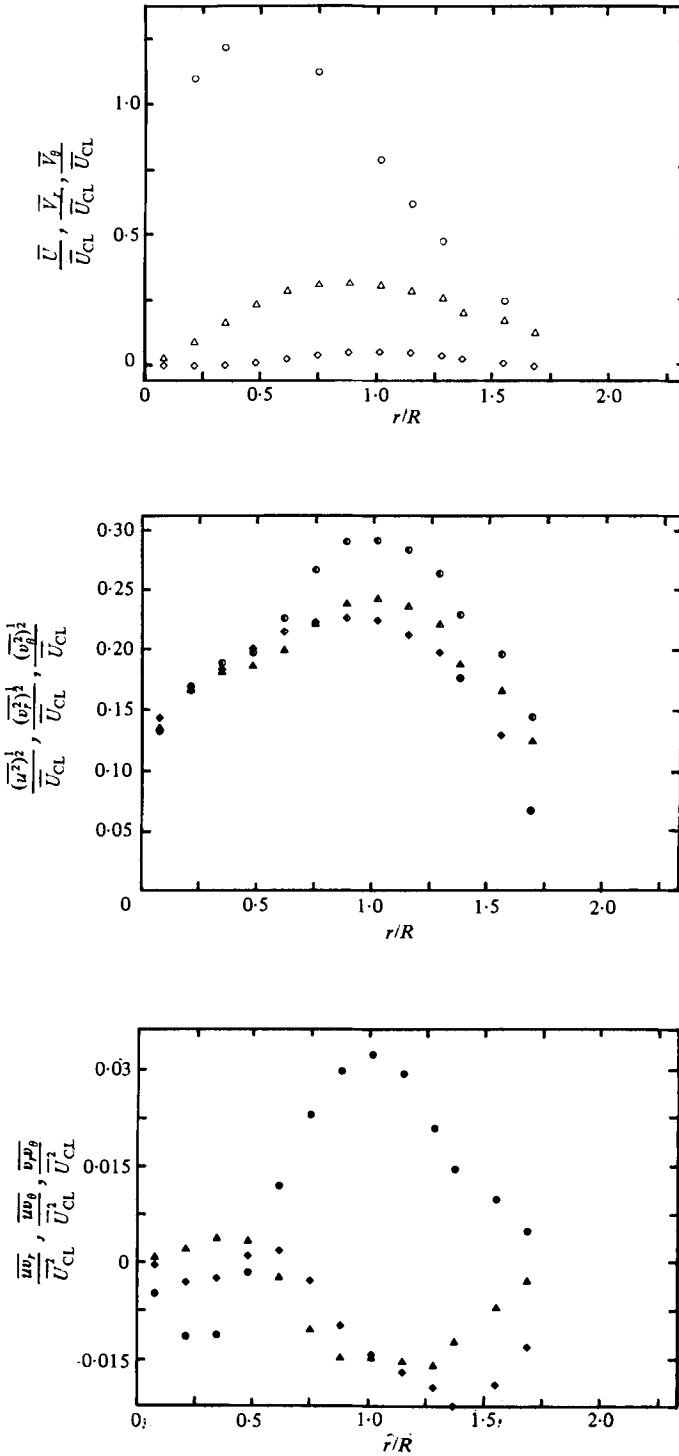
FIGURE 12. Radial profiles of mean velocities, turbulence intensities and Reynolds shear stresses, $x/D = 1\cdot50$, swirl number $= 0\cdot26$. Legend as for figure 10.
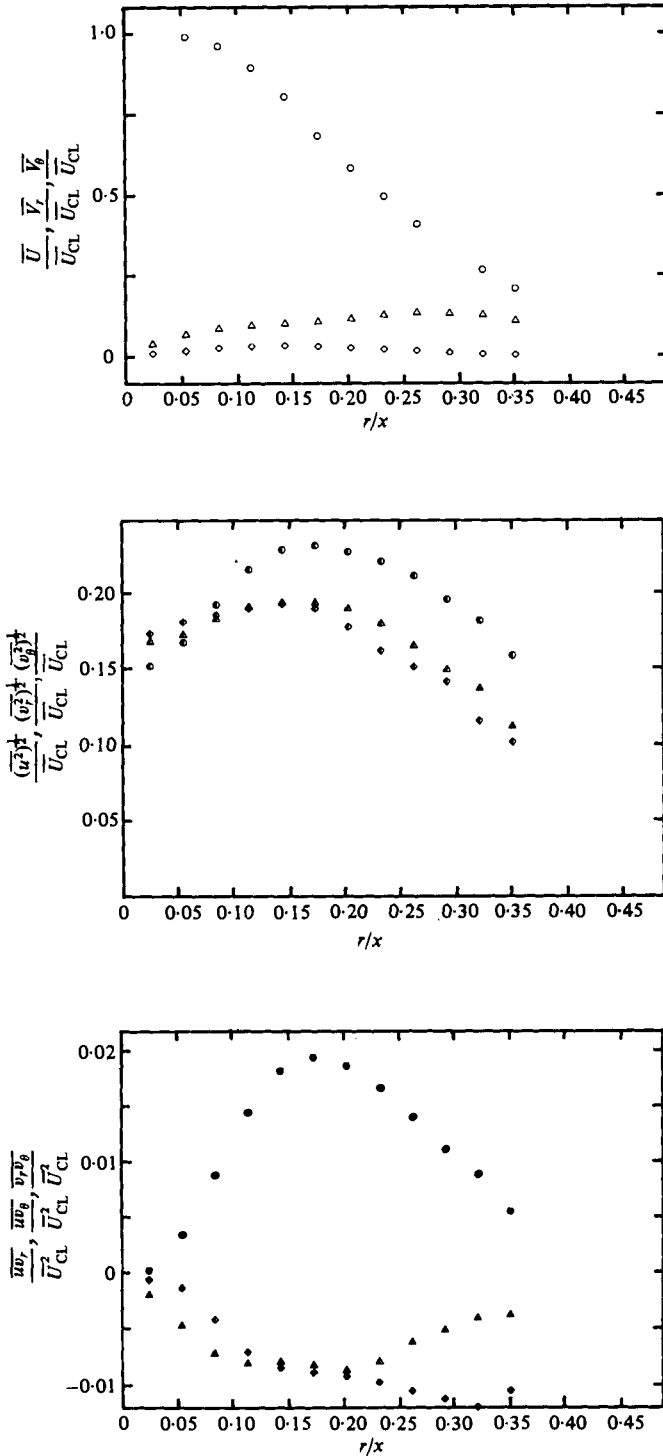
FIGURE 13. Radial profiles of mean velocities, turbulence intensities and Reynolds shear stresses, $x/D = 3\cdot00$, swirl number $= 0\cdot26$. Legend as for figure 10.
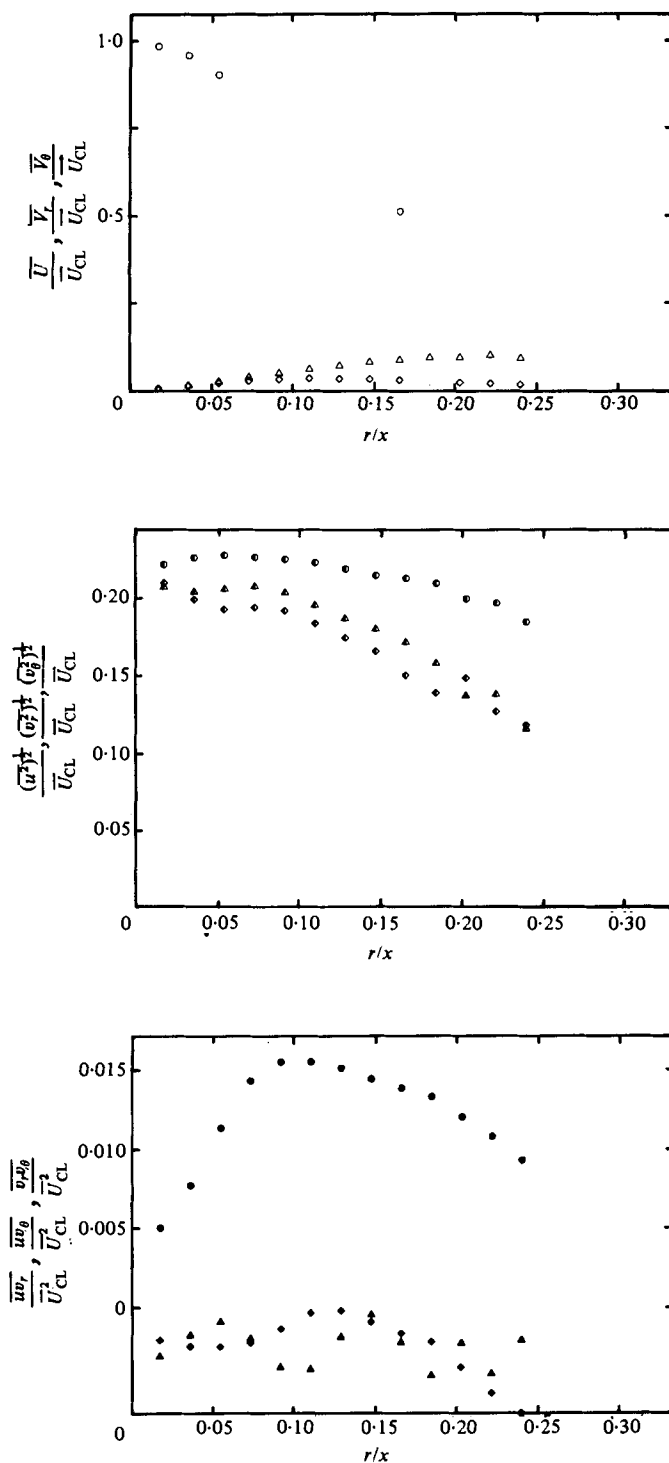
FIGURE 14. Radial profiles of mean velocities, turbulence intensities and Reynolds
shear stresses, $x/D = 6\cdot00$, swirl number $= 0\cdot26$. Legend as for figure 10.
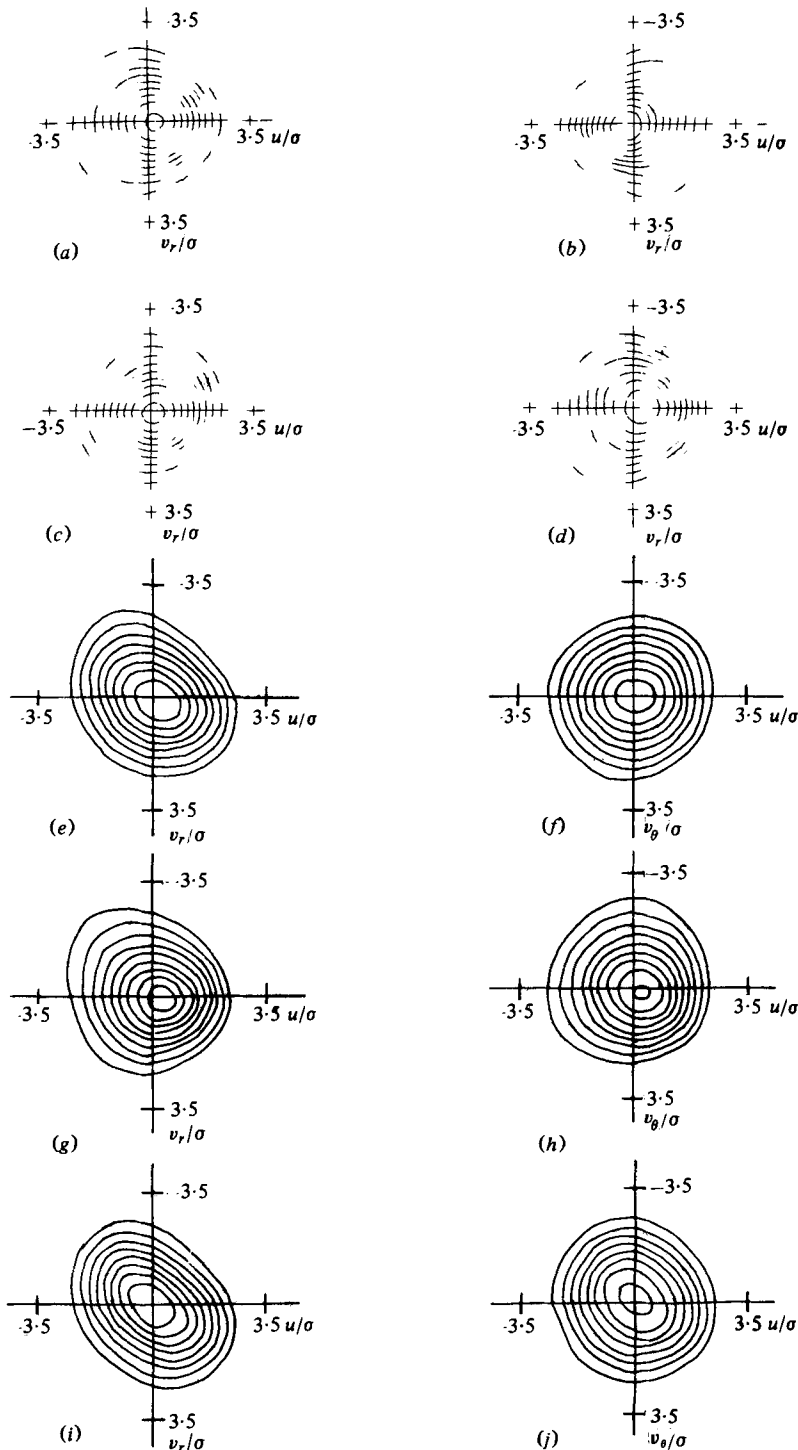
FIGURE 15. Two-dimensional probability density distributions $B(u, v_r)$ and $B(u, v_\theta)$, swirl number = 0·26. (a) $x/D = 0$, $r/R = 0$; (b) $x/D = 2·0$, $r/R = 0$; (c) $x/D = 3·0$, $r/R = 0$; (d) $x/D = 6·0$, $r/R = 0$; (e) $x/D = 0$, $r/R = 0·30$, $B(u, v_r)$; (f) $x/D = 0$, $r/R = 0·30$, $B(u, v_\theta)$; (g) $x/D = 0$, $r/R = 0·50$, $B(u, v_r)$; (h) $x/D = 0$, $r/R = 0·50$, $B(u, v_\theta)$; (i) $x/D = 0$, $r/R = 0·75$, $B(u, v_r)$; (j) $x/D = 0$, $r/R = 0·75$, $B(u, v_\theta)$.

direction, it is likely that turbulent transport does not play an important rôle in determining the shear stress. According to the previous argument, therefore, the Reynolds shear stress is locally determined. The distribution $B(u, v_\theta)$ is shown in figure 15 (f); as it refers to a location where there is no swirl, no correlation between u and v_θ exists, and an expected circular symmetry is obtained. Distributions 15 (g) and 15 (h) refer to a location near the inner wall of the annulus $(r/x = 0.5)$, where the stresses $\overline{uv_r}$ and $\overline{uv_\theta}$ are small; $B(u, v_r)$ shows a dependence of $\overline{uv_r}$ on transport from the outer region $(v_r < 0)$ by scales with a characteristic velocity lower than the local mean $(u < 0)$. This region is, therefore, affected mainly by diffusion of large scales and this is confirmed by distributions 15 (i) and 15 (j) which are associated with the outer edge of the annulus where the shape of the distributions suggests local production. Thus, for the annulus, turbulence is produced near the outer wall and moves towards the inner wall through turbulent mixing. This is consistent with the present swirl which is introduced at the outer wall and causes high turbulence levels that find their way to the inner regions by turbulent diffusion.

The distributions at locations further downstream are not represented here. They indicate that a pattern resembling self-preservation starts to emerge at $x/D = 1$ as opposed to $x/D = 6$ in the absence of swirl. The analysis of the distributions in the region of the wake of the inner pipe wall shows that vortex shedding still occurs but is less intense, partly because of the steeper velocity gradient on the side of the annulus generated by the backward-facing step located inside the swirling chamber.

4. Concluding remarks

In the Reynolds stress closures, such as that of Launder, Reece & Rodi (1975), the modelled quantities influenced by the large scales are the turbulent diffusion and the pressure-dependent terms. Diffusion is modelled with knowledge of the local values of Reynolds stresses and their spatial derivatives. The present evidence indicates that skewness (and hence turbulent diffusion) is dependent on the surrounding field where both the Reynolds stresses and their gradients can change. It is the only mechanism in the transport equations that explicitly contains third-order correlation and these are a 'first order' measure of the asymmetry in the probability density distributions. The diffusion model proposed by Bradshaw *et al.* (1967), which assumes the diffusive flux of energy to be proportional to energy times a diffusive velocity characteristic of the large scales of the motion, is more consistent with the present results. The diffusive velocity is taken as proportional to the square root of the average Reynolds shear stress across the field, on the grounds that the latter determines the production of the large eddies.

The pressure term contains two different types of contribution, one diffusive and another redistributive in nature. The influence of large scales on the diffusive contribution is unknown since there is no available information about the correlation between pressure and velocity fluctuations. The remaining pressure term is redistributive of turbulent kinetic energy and the only part in which the asymmetry of the fluctuation is relevant is the integral over space of the gradient of mean velocity multiplied by second derivatives of the second-order correlations. The integral nature of this term implies that only the symmetric part of the integrand contributes to redistribution. Thus the asymmetry of the large-scale fluctuations only contributes when combined

with the anti-symmetric part of the mean velocity gradient. It is therefore probable that the effects of the asymmetry of large scales on pressure redistribution is small.

The above arguments apply, in general, to situations that deviate from homogeneity. The flow situations considered here display additional features which cannot be represented in this way. One is the occurrence of vortex shedding in the wake of the inner pipe wall; the Reynolds stress closure, as it stands, cannot predict this feature. In addition, the intermittency of the fluctuations in the outer region of the jet is associated with strong asymmetry in the probability density distributions and, again, the Reynolds stress closure has no provisions to deal with the velocity correlations of odd order.

REFERENCES

BRADSHAW, P., FERRISS, D. H. & ATWELL, N. P. 1967 Calculations of boundary-layer development using the turbulence energy equation. *J. Fluid Mech.* **28**, 593.

CHAMPAGNE, F. H. & SLEICHER, C. A. 1967 Turbulence measurements with inclined hot wires. II. Hot-wire response equations. *J. Fluid Mech.* **28**, 177.

CHAMPAGNE, F. H. & WYGNANSKI, I. J. 1970 Co-axial turbulent jets. *Boeing Scientific Res. Labs Rep.* DI-82-0958.

CHIGIER, A. N. & BEER, J. M. 1964 The flow region near the nozzle in double concentric jets. *Trans. A.S.M.E.* D, *J. Basic Engng* **86**, 797.

CHIGIER, A. N. & CHERVINSKY, A. 1967 Experimental investigation of swirling vortex motions in jets. *Trans. A.S.M.E.* E, *J. Appl. Mech.* **89**, 443.

CHRISS, D. E. & PAULK, R. A. 1972 An experimental investigation of subsonic co-axial free turbulent mixing. *Arnold Engng Development Centre Rep.* AEDC-TR-71-236.

CRAYA, A. & DARRIGOL, M. 1967 Turbulent swirling jet. *Phys. Fluids Suppl.* **10**, S 197.

DURÃO, D. F. G. 1971 Turbulent mixing of co-axial jets. M.Sc. thesis, University of London.

DURÃO, D. F. G. & WHITELAW, J. H. 1973 Turbulent mixing in the developing region of co-axial jets. *J. Fluids Engng* **95**, 467.

FORSTALL, W. & SHAPIRO, A. H. 1950 Momentum and mass transfer in co-axial gas jets. *J. Appl. Mech.* **17**, 399.

HINZE, J. 1959 *Turbulence.* McGraw-Hill.

KAWAGUCHI, D. & SATO, G. T. 1971 Experimental investigation of premixed swirling jet flames (velocity and turbulence intensity of swirling air jets). *Bull. J.S.M.E.* **14**, 248.

LAUNDER, B. E., REECE, G. J. & RODI, W. 1975 Progress in the development of a Reynolds stress closure. *J. Fluid Mech.* **68**, 537.

MATSUMOTO, R., KYMOTO, K. & TSUCHIMOTO, N. 1973 A study of double concentric jets. *Bull. J.S.M.E.* **16**, 529.

RIBEIRO, M. M. 1972 Turbulent mixing of co-axial jets. M.Sc. thesis, University of London.

RIBEIRO, M. M. 1976 The turbulence structure of turbulent flows with and without swirl. Ph.D. thesis, University of London.

RIBEIRO, M. M. & WHITELAW, J. H. 1975 Statistical characteristics of a turbulent jet. *J. Fluid Mech.* **70**, 1.

RIBEIRO, M. M. & WHITELAW, J. H. 1976 Turbulent mixing of co-axial jets with particular reference to the near exit region. *J. Fluids Engng* **98**, 284.

RODI, W. 1971 A new method of analysing hot-wire signals in highly turbulent flow and its evaluation in a round jet. *Imperial College, Mech. Engng Dept. Rep.* ET/TN/B/10.

Rose, W. G. 1962 A swirling turbulent round jet. *J. Appl. Mech.* **29**, 615.

Townsend, A. A. 1956 *The structure of turbulent shear flows*. Cambridge University Press.

Tutu, N. K. & Chevray, R. 1975 Cross-wire anemometry in high-intensity turbulence. *J. Fluid Mech.* **71**, 785.